



# Evidence of active subglacial lakes under a slowly moving coastal region of the Antarctic Ice Sheet

Jennifer F. Arthur<sup>1</sup>, Calvin Shackleton<sup>1</sup>, Geir Moholdt<sup>1</sup>, Kenichi Matsuoka<sup>1</sup>, Jelte van Oostveen<sup>2</sup>

5 <sup>1</sup>Norwegian Polar Institute, 9296 Tromsø, Norway

<sup>2</sup>NORCE Norwegian Research Centre, 9294 Tromsø, Norway

*Correspondence to:* Jennifer Arthur (jennifer.arthur@npolar.no)

## Abstract

Active subglacial lakes beneath the Antarctic Ice Sheet provide insights into the dynamic subglacial environment, with implications for ice-sheet dynamics and mass balance. Most previously-identified lakes have been found upstream (>100 km) of fast-flowing glaciers in West Antarctica, and none in the coastal region of Dronning Maud Land (DML) in East Antarctica. The regional distribution and extent of lakes as well as their timescales and mechanisms of filling-draining activity remain poorly understood. We present local ice surface elevation changes in the coastal DML region that we interpret as unique evidence of seven active subglacial lakes located near the slowly-moving ice-sheet margin. Laser altimetry data from the ICESat-2 and ICESat satellites combined with multi-temporal REMA strips reveal that these lakes actively fill and drain over periods of several years. Stochastic analysis of subglacial water routing together with visible surface lineations on ice shelves indicate that these lakes discharge meltwater across the grounding line. Two lakes are within 15 km of the grounding line, while another three are within 54 km. Ice flows 17-172 m a<sup>-1</sup> near these lakes, much slower than the mean ice flow speed near other active lakes within 100 km of the grounding line (303 m a<sup>-1</sup>). Our observations add to a previously under-represented population of subglacial lakes that exist beneath slow-flowing ice near the ice sheet margin. Our results improve knowledge of subglacial meltwater dynamics and evolution in this region of East Antarctica and provide new observational data to refine subglacial hydrological models.

## 1 Introduction

Hydrologically-active subglacial lakes periodically store and release water beneath the Antarctic Ice Sheet and form a key component of the basal hydrological system. Active lakes are known to influence the dynamics of the overlying ice by reducing basal friction and periodically triggering short-term accelerations in ice flow (Stearns et al., 2008; Siegfried et al., 2016; Siegfried and Fricker, 2018; Andersen et al., 2023). Temporary accelerations in ice flow of up to ~10% have been linked to lake drainage events on Byrd Glacier, East Antarctica (Stearns et al., 2008), on Crane Glacier, the Antarctic Peninsula (Scambos et al., 2011), and on the Mercer and Whillans ice streams, West Antarctica (Siegfried et al., 2016). Individual active



30 subglacial lakes can range from  $\sim 5 \text{ km}^2$  to tens of square kilometres and have been shown to form connected networks over  
hundreds of kilometres (Fricker et al., 2007, 2009; Smith et al., 2009; Flament et al., 2014; Hodgson et al., 2022; Livingstone  
et al., 2022). Downstream subglacial water flow has been linked to cascading lake drainage events which transport excess  
water episodically towards the grounding line (Smith et al., 2017; Neckel et al., 2021). Meltwater outlets at the grounding line  
35 discharge freshwater into sub-ice-shelf cavities, which according to models could enhance ice-shelf basal melting (Carter and  
Fricker, 2017; Dow, 2022) and reduce sea-ice volume (Goldberg et al., 2023) and has also been shown to influence sediment  
fluxes (Lepp et al., 2022) and biogeochemical fluxes (Wadham et al., 2013). Therefore, observing active lakes using repeated  
satellite data is crucial to characterize subglacial hydrology and its impact on the ice-sheet-ocean system.

Over the past two decades, 140 active subglacial lakes have been detected underneath the Antarctic Ice Sheet using satellite  
40 data (Fig. 1, Livingstone et al., 2022). Satellite radar and laser altimetry (e.g., ESA's CryoSat-2 and NASA's Ice, Cloud and  
Land Elevation Satellites ICESat and ICESat-2) has successfully been used to identify localised ice surface elevation changes  
on annual to decadal timescales, interpreted as subglacial lake filling and draining activity and corresponding changes in lake  
volume (e.g., Fricker et al., 2007, 2010; Smith et al., 2009). Even finer patterns of centimetre-scale ice surface elevation  
changes have been identified using differential synthetic aperture radar interferometry (DInSAR) and interpreted as evidence  
45 for transient subglacial water transport (Gray et al., 2005; Neckel et al., 2021; Moon et al., 2022). Few active subglacial lakes  
have yet been reported beneath much of the grounded ice close to the Antarctic Ice Sheet margin (Livingstone et al., 2022).  
Consequently, little is known about the subglacial hydrology, water routing and the impact on local ice dynamics at the  
transition between grounded and floating ice in this region.

50 In this study, we build on previous work by providing a more complete inventory of active subglacial lakes by measuring ice  
surface elevation displacement observed from the laser altimeters onboard ICESat-2 between March 2019 and May 2023 and  
its predecessor ICESat between October 2003 and March 2009. We focus on the coastal Dronning Maud Land (DML) region  
of East Antarctica, where no active lakes have been identified previously (Fig. 1). We use ICESat and ICESat-2 elevation time  
series together with Reference Digital Elevation Model of Antarctica (REMA; Howat et al. 2019) strips to determine the  
55 temporal patterns of subglacial lake activity and estimate lake volume changes. We further estimate subglacial stream  
probability using water routing analyses derived from stochastic simulation (Shackleton et al., 2023) to assess upstream  
drainage basins and potential downstream impacts of the newly observed subglacial lakes. The combination of these datasets  
reveals seven previously-unreported active subglacial lakes that fill and drain over periods of multiple years and identifies the  
most probable pathways of meltwater released from lakes towards the grounding line. Our study provides insights into an  
60 active subglacial hydrological system and potential subglacial outlets close to the ice-sheet margin in eastern Dronning Maud  
Land. This can help to better constrain how subglacial lake activity regulates water availability and flow conditions under the  
ice sheet, as well as modifies ice-shelf cavity circulation and basal melting when meltwater is released at the grounding line.



## 2 Study Area, Data and Methods

### 2.1 Study Area

65 In the Dronning Maud Land (DML) sector of East Antarctica, previous work has identified a cluster of eight ice surface  
subsidence and uplift events between 2017-2020 ~160 km inland from Jutulstraumen Glacier using double differential  
synthetic aperture radar interferometry (DDInSAR) and ICESat-2 altimetry (Neckel et al., 2021). These vertical movements  
of the ice surface reached 14.4 cm and were interpreted as episodic subglacial lake drainage events with durations between 12  
70 days and ~1 year, indicating cascading subglacial water over a ~175 km flow path (Neckel et al., 2021). The DML coastal  
region is also characterized by sparse radar-detected, stable subglacial lakes. Goeller et al. (2016) found 33 locations with  
distinct characteristics in airborne ice-penetrating radar data that can be interpreted as subglacial lakes 40 km or further inland  
from the grounding line (7.2-16.2° E). So far, no active subglacial lakes have been recorded in the coastal region of DML  
within 160 km of the ice margin. We focus on the coastal region of grounded ice in DML, extending along the Princess Astrid  
Coast and the Princess Ragnhild Coast up until the Roi Baudouin Ice Shelf (69° S to 72° S and 33° W to 6° E; Fig. 1). There  
75 are ~13 fast-flowing outlet glaciers along this coast (88 – 281 m a<sup>-1</sup>), which are surrounded by slowly moving ice (2-30 m a<sup>-1</sup>,  
Gardner et al., 2018). Grounded ice in this region of the ice sheet lies largely below present-day sea level (Morlighem et al.,  
2020; Frémand et al., 2023, Fig. 1). Satellite altimetry from ICESat/ICESat-2 has recorded significant ice-sheet thickening in  
DML over the last two decades (Smith et al. 2020) due to high snowfall rates (e.g. Boening et al., 2012).

### 2.2 Satellite Altimetry

#### 80 2.2.1 ICESat-2

NASA's next generation Ice, Cloud, and land Elevation satellite (ICESat-2) is a photon-counting laser altimeter providing  
repeat-pass ice surface height measurements every 91 days (Markus et al., 2017). The Advanced Topographic Laser Altimeter  
System (ATLAS) on board ICESat-2 continuously profiles the Earth's surface along its 1387 reference ground tracks (RGTs)  
using six laser beams, which measure three pairs of tracks, with each pair separated by 3.3 km. The beams within each pair  
85 are separated by ~90 m. Elevation-change data in this paper are based on release 6 of the ICESat-2 Level 3b Slope-Corrected  
Land Ice Height time series (ATL11) product (Smith et al., 2022) which became available in August 2023. We used the ATL11  
data spanning between April 2019 and April 2023, for which the geolocation of each beam is accurately determined (Smith et  
al., 2023). All previous studies detecting subglacial lakes in Antarctica from ICESat-2 have used the lower-level ICESat-2  
ATL06 product, which provides geolocated, land-ice surface heights that are corrected for geophysical impacts and instrument  
90 bias (e.g. Siegfried and Fricker, 2021; Neckel et al., 2021; Fan et al., 2022).

A main difference between ATL06 and ATL11 is that ATL06 elevations require slope correction using a DEM or data-fitted  
reference surface when comparing repeat-tracks, whereas this is already done as part of the ATL11 processing, providing time  
series of along-track ice surface heights that are slope-corrected onto a reference pair track (RPT) for each cycle and are



95 accurate to  $<0.07$  m (Smith et al., 2019; Brunt et al., 2021). In this way, ATL11 height estimates correct ATL06 heights for  
the combined effect of small cross-track offsets (up to  $\sim 130$  m) between repeat measurements and sub-kilometre and surface  
topography around fit centres. The ATL11 product has so far been used in Antarctica for assessing the impact of net snow  
accumulation variability on observed surface height change (Medley et al., 2022) and for investigating ice-shelf basal channel  
morphology at the Kamb Ice Stream grounding line (Whiteford et al., 2022). Over the Greenland Ice Sheet, ATL11 has been  
100 used for evaluating spatial patterns of surface mass balance and firn densification (Smith et al., 2023) and for investigating  
subglacial lake activity beneath the ablation zone (Fan et al., 2023).

Two types of height error estimates are provided with ATL11. One is random per-point estimates ( $h_{corr\_sigma}$ ), which  
include the errors related to the accuracy of the reference surface and the precision of the ICESat-2 range estimates and are  
105 uncorrelated between adjacent reference points (Smith et al., 2023). The other is systematic error estimates  
( $h_{corr\_sigma\_systematic}$ ), which include the slope-dependent impact of geolocation errors that are correlated along each  
track. We find maximum per-point error and systematic error in the corrected surface heights of 14.9 cm and 14.5 cm  
respectively for the ICESat-2 data we analyse here. These maximum values are higher than reported per-point errors in the  
ice-sheet interior of 1-2 cm, because rougher, steeper surfaces towards the coast typically degrade the instrument precision and  
110 slope correction (Smith et al., 2023). However, the mean per-point and systematic errors for the ICESat-2 data analysed here  
are still as low as 2.7 cm and 5.3 cm, respectively.

To investigate subglacial lake drainage and filling patterns, we followed the approach of calculating repeat-track elevation  
anomalies (Fricker et al., 2014; Neckel et al., 2021; Siegfried and Fricker, 2018; 2021). We first removed poor-quality surface  
115 elevations, potentially caused by cloud cover, blowing snow or background photon clustering based on ATL11's overall quality  
summary flag ( $atl11\_qual\_summary == 0$ ) (Siegfried and Fricker, 2021). Previous studies have calculated elevation anomalies  
with respect to a DEM or other reference surface (Fricker et al., 2014; Neckel et al., 2021). Using ATL11, we assessed ice  
surface elevation changes directly with respect to the start of our observation period (April 2019) by calculating elevation  
anomalies ( $dh$ ) for each ATL11 point along every RGT relative to the first available cycle ( $h_0$ ) using:  $dh = h - h_0$ , where  $h$  is  
120 ice surface elevation. We calculated time series of elevation anomalies along each RGT.

### 2.2.2 ICESat

NASA's Ice, Cloud, and land Elevation satellite (ICESat) was a laser altimeter providing ice surface height measurements in  
footprints of  $\sim 65$  m-diameter separated by  $\sim 172$  m along its RGTs (Zwally et al., 2002). We used ICESat GLA12 ice-sheet  
product version 34 collected between February 2003 and October 2009 to derive elevation changes. ICESat RGTs were  
125 typically repeated within  $\sim 150$  m cross-track distance, and vertically accurate within a few tens of centimetres depending on  
surface slope (Brenner et al., 2007; Kohler et al., 2012). ICESat crossover errors (i.e. at the point between successive ascending  
and descending passes over the same location) have been estimated between 7.5 cm for flat surfaces to 20 cm for  $1^\circ$  slopes,

meaning most errors are  $<0.1$  m given the minimal surface slopes over most of the Antarctic Ice Sheet (Smith et al., 2009). The GLA12 product was used for compiling the first comprehensive Antarctic inventory of 124 active subglacial lakes north of  $86^\circ$  S, demonstrating short-term basal hydrologic evolution of lakes throughout Antarctica (Smith et al., 2017).

We estimated along-track elevation changes from GLA12 following the approach of Moholdt et al. (2010) by fitting surface planes to 700 m segments of repeat track data, determining surface elevation anomalies for all laser footprints with respect to the plane fit. Outlier points with elevation anomalies  $>10$  m, for example due to cloud scattering or rough topography, were iteratively removed in the plane-fit processing. This threshold was set higher than the expected elevation changes due to subglacial lake activity, in order to not remove such data. We further neglected potential long-term elevation changes due to surface mass balance and large-scale ice dynamics in the plane fitting as these are generally small in the study region and could interfere with changes due to subglacial lake activity.

### 2.3 Subglacial lake detection

Previous studies have identified lakes based on thresholds between  $\pm 0.1$ - $0.5$  m for spatially-coherent elevation anomalies using ICESat (Fricker et al., 2007, 2014; Smith et al., 2009) and Cryosat-2 (Kim et al., 2016; Smith et al., 2017, Malczyk et al., 2020). We adapted these previous approaches to our coastal study region, which is characterized by high slope and roughness, by identifying potential areas of subglacial lake activity from ICESat/ICESat-2 repeat-tracks with significant ( $\pm 1$  m) elevation anomalies over a distance of  $\geq 1$  km. The elevation anomaly patterns over these areas were then manually examined to assess whether these appeared to reflect lake activity (i.e., arc-shaped profiles of draining and/or filling) or if they were in, for example, highly-crevassed or sloping regions where unresolved rough topography is likely to dominate the signal. We found using a  $\pm 1$  m threshold applied to elevation anomalies relative to the start of our observation period best highlighted and distinguished substantial localised anomalies from background along-track elevation changes and noise, whereas lower thresholds (e.g.  $\pm 0.5$  m) included surface elevation change signals that are unlikely to be related to subglacial lake activity.

### 2.4 REMA Strip Differencing and lake outlines

To further investigate subglacial lake activity and spatial extents, we used high-resolution stereoscopic data from REMA (Howat et al., 2019) over the locations where we detected ICESat-2 anomalies in surface elevation change. We differenced available DEM strips with 2-m map cells acquired between September 2015 and December 2021 that intersected regions with elevation anomalies identified in ICESat/ICESat-2 data to calculate spatial ice surface height changes over three suspected lakes (L1, R1, R2: Table 1). The number of useable DEM strips (i.e. partially or fully covering each lake) in any given year averaged between 1 and 3 strips per lake (Supplementary Fig. 1). The strip DEMs are generated by applying fully-automated, stereo auto-correlation techniques to overlapping pairs of high-resolution optical satellite images, using the open-source Surface Extraction from TIN-based Searchspace Minimization (SETSM) software (Howat et al., 2019). Individual 2-m REMA strips are not co-registered to satellite altimetry, unlike the REMA mosaic (Howat et al., 2019), meaning that relative elevation



160 within a strip is precise but has low absolute accuracy (Hodgson et al., 2022). To increase absolute accuracy, DEM strips can  
be coregistered using static reference points, typically rock outcrops (Shean et al., 2019). The strips we used do not include  
any outcrops, so instead we estimated and removed vertical elevation biases by using the temporally closest overlapping  
ICESat-2 track within +/- 100 days of the DEM strip acquisition date (Chartrand and Howat, 2019; Priergaard Zinck et al.,  
2023). This time restriction ensures that the ICESat-2 elevations are representative of elevations during strip acquisition,  
165 although we acknowledge that some lake filling or drainage could still occur within this time period.

Of the ten DEM strips that intersected the seven potential areas of subglacial lake activity we identified, six strips were  
vertically co-registered to ICESat-2 elevations (Supplementary Table 1). The other four strips were not co-registered due to  
lacking contemporaneous ICESat-2 data, but were still included to provide further insight into the lake activity of Lakes L1  
170 and R1 (Supplementary Fig. 2). In these cases, the remaining vertical biases are reflected in near-constant elevation differences  
outside of the active lake areas. Static lake boundaries were digitized from the pattern of elevation anomalies in the REMA  
difference maps (Lakes L1, R1 and R2). We were unable to estimate the areas of four lakes (M1, M2, V1, R3) because the  
REMA strip differences did not show any significant elevation anomalies. For illustrative purposes, we still sketched  
speculative lake boundaries for these four lakes (Fig. 2d-e) based on ICESat-2 elevation anomaly locations and the REMA  
175 mosaic hillshade (Howat et al., 2019).

## 2.5 Subglacial lake volume changes and recharge rates

To estimate lake volume changes, we multiplied the REMA-derived lake areas (where available) with the altimetry-based  
median elevation anomaly within this lake boundary for each repeat track (Smith et al., 2009; Carter et al., 2013). We  
approximated subglacial water flux by the volume change corresponding to ice surface uplift/deflation over time (Malczyk et  
180 al., 2020, 2023). Recharge rates (reported as annual water supply to each lake) were estimated by applying linear regression  
against volume change and time during the refilling (inter-drainage) period, following Malczyk et al. (2020). We were unable  
to estimate volume changes for the five lakes without a clear or complete lake boundary in the REMA data. In the absence of  
further constraints on lake extent changes over time, we assume a constant lake area throughout the fill-drain cycle and a  
constant overlying ice thickness (Fricker and Scambos, 2009), even though migrating lake boundaries through fill-drain cycles  
185 can impact the estimated lake volume changes (Siegfried and Fricker, 2021).

## 2.6 Hydropotential Subglacial Water Flow Mapping

To interpret the satellite-detected lake activity in the context of the broader hydrological system under the ice sheet, we mapped  
potential subglacial water drainage pathways and their uncertainty based on an ensemble of water routing analyses following  
the approach of Shackleton et al., (2023). We made a 1 km grid for the DML region, limited to ca. <math>73^\circ</math> south to save  
190 computation time, and calculated the probability of each grid cell to contain subglacial streams. We did this by first generating  
50 equally-likely bed topography grids with continuous, realistic roughness simulated between radar-derived ice thickness



measurements using a sequential Gaussian simulation algorithm (MacKie et al., 2023). Ice thickness data from Frémand et al. (2023) were used as a basis for the simulations, after filtering out surveys conducted before 1990 which have limited locational accuracy, and converting to bed elevation data by subtracting it from extracted surface elevations of the 500 m REMA mosaic product (Howat et al. 2019). We also added elevation data from rock outcrops at pixel centroids of the REMA 500 m grid (Howat et al. 2019). We divided the region into 12 clusters using a k-means clustering algorithm and calculated the experimental variogram for measurements which we used to fit a statistical model representing measurement variance at increasing lag distances in each regional cluster. This was done to sequentially simulate values between measurements along a randomized path over the domain by picking from a Gaussian distribution conditioned at each grid cell by the closest 50 bed elevation measurements and modelled variance. The resulting ensemble of 50 bed elevation grids were then used to estimate subglacial hydraulic potential ( $\phi$ ) following Shreve (1972). We also used the median absolute deviation (MAD) between the 50 simulated bed elevation grids as a measure of bed elevation uncertainty. Low MAD is associated to regions with a high data density and lower basal roughness, whereas high MAD occurs for large distances between survey profiles and in regions with high basal roughness where there is greater potential for variability between measurements. Figure 1b shows where the MAD is lower than 100 m, indicating regions of relatively low bed uncertainty and higher confidence in simulated subglacial water routing.

We assumed that water pressure equals ice overburden pressure, and calculated water routing for hydraulic potential gradients based on a depression-filled bed topography using a  $D_{\infty}$  algorithm (Tarboton, 1997). Subglacial stream probability was calculated based on predicted streams over the ensemble of simulated bed topography. This method provides uncertainty-constrained water routing predictions where uncertainty can be sourced either from a lack of measurements (i.e. topography is not known well-enough), lack of strong topographic control on water flow, or both. Low probability streams are therefore associated to regions with sparse data or in flat areas where water routing is sensitive to minor fluctuations in bed elevation between simulations. We further estimated the average upstream subglacial hydrological catchment area for each altimetry-detected lake, based on the average upstream watershed area generated from our water routing analyses and derived catchment boundary probabilities based on the 50 stochastic simulations (Supplementary Fig. 6).

### 3 Results

#### 3.1 Observed ice surface displacements and interpreted lake activity

We identify seven locations with significant ( $>1$  m) anomalous, repeated surface elevation changes over distances of a kilometre or more from ICESat/ICESat-2 repeat tracks, which we interpret as active subglacial lakes. Lake R1 is located 19 km upstream from the Roi Baudouin Ice Shelf grounding line and is crossed by two intersecting ICESat-2 tracks and one ICESat track that all show a  $\sim 5$ -km wide elevation anomaly (Fig. 2a, Table 1). Lake L1 is 32 km upstream of the Lazarev Ice Shelf and is crossed by two ICESat tracks and two ICESat-2 tracks (Fig. 2b). Lake R2 is 115 km inland from the Roi Baudouin





Ice Shelf and is crossed by only one ICESat-2 track (Fig. 2c). Lake V1 is located 54 km upstream of the Vigridisen Ice Shelf  
225 and is crossed by two intersecting ICESat-2 tracks (Fig. 2d). Lakes M1 and M2 are only 10 km apart, and 5 km and 15 km  
upstream of the Muninisen Ice Shelf, respectively (Fig. 2e). Lastly, Lake R3 is 136 km inland from the Roi Baudouin Ice Shelf  
and is crossed by one track (Fig. 2f), which shows a ~7-km wide elevation anomaly (Supplementary Fig. 3d).

Following Smith et al. (2009), we classify ‘high-confidence’ active lakes as being detected from elevation anomalies in at least  
230 two intersecting reference tracks, and lakes that are only identified from one satellite altimetry track as ‘provisionally active’.  
By this definition, five of the lakes (R1, L1, V1, M1 and M2) are classified as high-confidence, and two (R2 and R3) as  
provisionally active. However, we can independently detect localised elevation anomalies over Lake R2 from REMA strip  
differencing, supporting that this is an actively filling and draining lake. Three of the seven lakes were confirmed and delineated  
by REMA strip differencing during 2019-2021 (Fig. 4; L1, R1, R2) and two of these also had intersecting ICESat tracks to  
235 extend the change record back to 2003-2009 (Fig. 3 and 5; L1 and R1). Their lake areas range from 21.5 to 40.1 km<sup>2</sup> (Table  
1). The other four lakes (V1, M1, M2, R3) had no ICESat data and no detectable change between REMA strips, likely due to  
negligible elevation changes between the dates covered by the strips.

All seven active lakes are located below sea level and beneath ice thicknesses of 800-1500 m (Fig. 1b). These lakes are typically  
240 located in relatively slow-flowing regions: two lakes under 20 m a<sup>-1</sup>, three lakes between 60-90 m a<sup>-1</sup>, and two beneath slightly  
faster-flowing tributaries at 152 and 172 m a<sup>-1</sup> (Fig. 1b, Table 1). The lakes located close to ice flow divides are beneath  
especially slow-flowing ice, for example Lake L1 (Fig. 1b, Table 1). The lakes upstream of Vigridisen and Muninisen ice  
shelves are located beneath faster-flowing outlet glaciers (up to 170 m a<sup>-1</sup>; Gardner et al., 2018).

245 We assume a one-to-one ratio between ice surface elevation changes and lake volumetric change, following previous studies  
in Antarctica and Greenland (Smith et al., 2009, Malczyk et al., 2023, Fan et al., 2023). It is possible that some ice surface  
uplift and subsidence could be influenced by ice-flow dynamics, blowing snow and changes in basal traction, resulting in  
misinterpretation as subglacial lake activity (Sergienko et al., 2007; Humbert et al., 2018), so this relationship lacks precise  
quantification (Siegfried and Fricker, 2018). For example, in fast-flowing regions, surface-elevation changes can reflect ice-  
250 flow changes triggered by water displacement at the bed during lake drainage (Smith et al., 2017). Most the lakes in this study  
are beneath relatively slow-flowing ice (< 100 m a<sup>-1</sup>), making it unlikely that observed ice surface changes resulted from ice  
flowing into basal topographic depressions. The patterns of surface elevation change we observe are characteristic of subglacial  
lake drainage (i.e. deepening towards the lake centre) and lack uplift near localised subsidence, which can be a signal of ice  
dynamical changes (Carter and Fricker, 2012). We also note that lake widths (inferred from elevation anomaly widths) are  
255 large relative to ice thickness (e.g. L1: ~8.5 ice thicknesses, R1: ~4 ice thicknesses), whereas ice-dynamical effects tend to  
dominate only when lakes are small relative to ice thickness (Fricker and Scambos, 2009). Ice surface changes over our newly-  
identified lakes (up to 4.5 m) are much larger than those related to wind-driven snow redistribution and firn compaction,





typically  $<0.5 \text{ m a}^{-1}$  based on repeat-track elevation changes elsewhere in the region. Furthermore, the spatial co-occurrence between altimetry- and REMA-derived elevation anomalies and predicted subglacial stream locations (Section 3.3) gives us  
260 confidence that subglacial meltwater drains towards the observed lakes and that elevation changes are therefore due to subglacial lake activity rather than other surface changes. Therefore, we conclude that the ice surface elevation changes we observe reflect changes in water volume rather than ice dynamics and surface processes, although we acknowledge that actual lake volume changes are still uncertain due to potential migration of lakeshore boundaries through fill-drain cycles (Siegfried and Fricker, 2021).

### 265 **3.1.1 Lake L1 upstream of Lazarevisen**

Over Lake L1 we find steady ice surface subsidence between August 2020 until May 2023 (Fig. 3d-f), suggesting a lake drainage event over a period of at least 2 years and 8 months. This is preceded by a slight ice surface uplift between May 2019 and May 2020, indicating lake refilling. REMA data show slight subsidence beside these tracks during September 2015 – December 2016 and January 2020 – February 2021, suggesting overall lake volume loss during these two periods (Fig. 4c,  
270 Supplementary Fig. 1b). This is consistent with the time series of lake volume derived from ICESat-2, showing the lake steadily draining between May 2020 and May 2023 (Fig. 3f). Elevation anomalies along the two intersecting ICESat tracks continue for 5 km along Track 134 and 7 km along Track 215, reaching a maximum value of 3 m at the lake centre (Fig. 3d-e, Supplementary Fig. 4a). The lake-averaged elevation anomaly time series over Lake L1 (Fig. 5) reveals positive elevation anomalies from November 2003 to March 2007 followed by a large ( $> 3 \text{ m}$ ) subsidence over the next 1 year and 8 months,  
275 indicating lake drainage. Ice surface displacements show a distinct minimum at the lake centre that tapers out towards the lake edges.

### **3.1.2 Lakes R1, R2 and R3 upstream of Roi Baudouin**

The time series of elevation anomalies from ICESat-2, ICESat and REMA strip differencing show variable drain and/or fill patterns for these three lakes over the past two decades (Figs 3 and 5). The elevation time series for Lake R1 shows negative  
280 anomalies up to  $-2.4 \text{ m}$  in December 2019, followed by a gradual elevation increase to up to  $4.5 \text{ m}$  in March 2023 (Fig. 3a-b). We interpret this as ice surface subsidence in response to lake drainage, followed by uplift in response to the lake filling over the next 3 years and 5 months. This is consistent with observed elevation gain (lake filling) from REMA differencing between October 2019 and January 2021 (Fig. 4a). Earlier REMA data indicate a slight subsidence (lake drainage) between December 2016 and December 2017 (Supplementary Fig. 2a), just ahead of the ICESat-2 observed subsidence in 2019. Time series of  
285 lake volume change shows the lake steadily filling between April 2019 and March 2022 (Fig 3c). More than a decade earlier, ICESat repeat tracks show a steady subsidence across the same area between 2003 and 2009 (Fig. 5, Supplementary Fig. 4b), which we interpret as lake draining. ICESat-2 data show that Lake R2 was draining between May 2019 and April 2021, and has since been filling through to April 2023 (Supplementary Fig. 3c). The shape of the lake can be seen from a distinct pattern



of uplift between two REMA strips from January 2021 and December 2022 (Fig. 4b). Lastly, over Lake R3 we find continuous  
290 ice surface uplift from August 2019 to April 2023 in response to lake filling (Fig. 5).

### 3.1.3 Lakes V1, M1, M2 upstream of Vigridisen and Muninisen

We record up to -1.6 m ice surface subsidence over Lake V1 from August 2019 to May 2023, which we interpret as continuous  
lake drainage (Fig. 5, Supplementary Fig. 3a). We find continuous ice surface uplift along a ~2.5-km wide zone of Lake M1  
from May 2019 until May 2023, suggesting lake filling over 4 years (Fig. 5, Supplementary Fig. 3b). Likewise at Lake M2,  
295 we found continuous ice surface uplift along a ~3-km wide elevation anomaly from September 2019 to June 2023, indicating  
lake refilling during this ~3 year and 8-month period (Fig. 5, Supplementary Fig. 3b). There is a striking coherence between  
the filling rates of these two lakes during the ICESat-2 period. Without any further intersecting altimetry tracks or clear change  
patterns in REMA strips for these lakes, it is difficult to constrain their areas and volume changes. The lack of significant  
localised elevation changes from REMA differencing could be because they had just drained and not yet refilled in the period  
300 covered by the DEM strips, or that draining and refilling have roughly balanced each other.

### 3.2 Subglacial lake volume changes, recharge rates and water flux

We calculated annual water supply and recharge rates for lakes R1 and L1, where lake boundaries were fully delineated from  
REMA strip differencing (Fig. 4). Lake R1 steadily gained volume from December 2019 to January 2023 before starting to  
drain (Fig. 3c, Fig 5). The associated volume gain of 0.13 km<sup>3</sup> over 3.5 years corresponds to a yearly recharge rate of 0.03 km<sup>3</sup>  
305 a<sup>-1</sup>. Lake L1 gained 0.01 km<sup>3</sup> volume between February 2020 and August 2020 before starting to drain until May 2023 (Fig.  
3f). During this half-year period, Lake L1 recharged at a rate of 0.02 km<sup>3</sup> a<sup>-1</sup>. Similarly-sized active lakes have been suggested  
to recharge at similar rates to those reported here, for example Lake Cook E2 (46 km<sup>2</sup>, 0.05 km<sup>3</sup> a<sup>-1</sup>) and Lake Whillans 2b (25  
km<sup>2</sup>, 0.02 km<sup>3</sup> a<sup>-1</sup>) (Li et al., 2020; Malczyk et al., 2020). Our estimated lake volume gains and losses are of similar magnitude  
to the median lake volume change of ~0.12 km<sup>3</sup> for 140 active lakes around Antarctica based on their surface elevation histories  
310 (Livingstone et al., 2022). However, since we are unable to capture a full drainage or filling cycle for most lakes, actual lake  
volume changes between minimum and maximum states are likely higher than what we can capture.

To approximate the subglacial meltwater flux entering/leaving the largest lake we detected (Lake L1), we calculated the rate  
of volume change corresponding to ice surface uplift/deflation over time (Malczyk et al., 2020). We use Lake L1 as an example  
315 for estimating water flux, as it is located close to the ice margin where topographic uncertainty is relatively low, and has one  
of the smallest mean upstream catchment areas (0.9 x 10<sup>4</sup> km<sup>2</sup>, Table 1). Average subglacial water flux was 4.9 m<sup>3</sup> s<sup>-1</sup> between  
November 2003 and May 2023. For comparison, Malczyk et al. (2020) estimated an average water flux of 141 m<sup>3</sup> s<sup>-1</sup> in 2013  
for a network of active lakes upstream of Thwaites Glacier (Thw<sub>70</sub>, Thw<sub>124</sub>, Thw<sub>142</sub> and Thw<sub>170</sub>). Modelled upstream melt  
supplies to their lake network range from 0.04-0.17 km<sup>3</sup> a<sup>-1</sup> (1.3-5.4 m<sup>3</sup> s<sup>-1</sup>) although these lakes are considerably larger than  
320 those in our study (up to 484 km<sup>2</sup>; Smith et al., 2017). In our water flux estimations, we assume no lake outflow during lake



filling, though it is possible a lake could increase in volume whilst discharging water downstream if a high lake influx exceeds lake outflow (Carter and Fricker, 2012). These assumptions mean that our estimated water flux is likely to be a minimum estimate.

### 3.3 Subglacial water flow

325 We simulated an ensemble of 50 equally-likely bed elevation grids using sequential Gaussian simulation. The resulting grids are consistent along survey profiles and have continuous, regionally representative roughness simulated between measurements. Throughout the ensemble, water routing analyses predict dendritic networks of subglacial streams routing water from inland towards the grounding line (Supplementary Fig. 5). This broad pattern of drainage remains consistent over the ensemble, but the kilometer-scale routing of meltwater varies. Stream probability maps (Fig. 1a) show water flow predictions  
330 strongly controlled by bed topography in the inland mountain regions where radar measurements are limited but nevertheless outcrop surface elevation data help constrain the bed topography. High stream probability coincides with dense radar survey coverage, for example surrounding the Nivlisen Ice Shelf, showing the impact of data density on reducing water routing uncertainty. Lower stream probability regions that resemble diffuse, spatially-distributed streams occur between higher-probability streams, for example inland of the Roi Baudouin Ice Shelf eastward of 27° E (Fig. 6e) and inland of the Muninisen  
335 Ice Shelf, often coinciding with widely-spaced radar survey profiles. Other regions show inconsistent water routing despite regularly-spaced radar profiles, such as within 50 km of the Vigridisen grounding line (Fig. 1a). This reflects an absence of strong topographic features that control the routing of water, meaning small differences in simulated topography over the ensemble can reroute water and lead to inconsistent water routing and more diffuse stream predictions.

340 We compared our lake observations with the subglacial drainage patterns and found good spatial correspondence over some of the lakes. Predicted water routing shows direct drainage to the western Roi Baudouin Ice Shelf grounding line and identifies likely subglacial outlet locations (Fig. 6a). Lake R1 aligns with several known subglacial water conduits detected in airborne ice-penetrating radar data that align with two sub-ice-shelf channels (Fig. 6a, Drews et al., 2015; 2017; 2020). This agreement indicates that Lake R1 is likely to be discharging subglacial meltwater directly into the ice-shelf cavity through a channelized  
345 subglacial conduit system and could contribute to a meltwater plume that forms the sub-ice-shelf channel. However, Lake R1 is 6 km from the closest radar survey profile, and our subglacial stream probabilities highlight that precise drainage routes are less certain here since topographic uncertainty is over 125 m in the middle of adjacent radar survey profiles (Fig. 6a). Given the topographic uncertainty in this region, we cannot rule out the potential for lake drainage towards different outlets, for example if ephemeral subglacial channels close between drainage events. Several ice-shelf channels on Roi Baudouin aligned  
350 to ice flow direction correspond with the predicted subglacial meltwater outlets beneath the grounded ice sheet and align with the location of Lakes R2 and R3 (Fig. 6e). Therefore, Lakes R2 and R3 could discharge basal water that is routed towards multiple subglacial outlets at the Roi Baudouin grounding line.



Further west, the probability map of subglacial drainage catchments (Supplementary Fig. 6) shows with high confidence that  
355 an extensive catchment of minimum 19,000 km<sup>2</sup> is draining towards Lake V1. Downstream water routing predictions vary too  
much at the kilometre-scale to conclusively determine ice margin outlet locations, and water routing shows drainage towards  
the grounding lines of either Vigridisen Ice Shelf or the neighbouring Fimbulisen Ice Shelf (Fig. 6b). Inland of Lazarevisen  
Ice Shelf, predicted subglacial stream and outlet locations become more uncertain, reflecting sparser radar profile spacing (up  
to 19 km), but suggest Lake L1 likely discharges meltwater to the Lazarevisen Ice Shelf grounding line (Fig. 6c). Our water  
360 routing analyses also predicts high-probability streams connecting Lakes M1 and M2, suggesting interconnected lakes which  
drain directly into the ice-shelf cavity (Fig. 6d). The predicted subglacial outlet here is close to several sub-ice-shelf channels,  
indicating Lakes M1 and M2 feed a persistent sub-shelf channel when they drain.

## 4 Discussion

### 4.1 Lake distributions at the Antarctic ice-sheet margin

365 We identify seven previously undocumented active subglacial lakes in coastal DML at six localities in five different drainage  
basins and within 5 km of the ice-sheet grounding line, feeding into separate ice shelves (Fig. 1a). The combination of ICESat,  
ICESat-2 and REMA observations presented here build upon large-scale repeat satellite altimetry studies of hydrologically-  
active subglacial lakes elsewhere in Antarctica (e.g., Fricker et al., 2007, 2009; Smith et al., 2009; Siegfried and Fricker, 2021).  
Only ten active lakes have been identified previously within 50 km of the Antarctic-wide grounding line for the rest of  
370 Antarctica (Livingstone et al., 2022). These ten known lakes nearby the grounding line are found on the Antarctic Peninsula  
(1 lake), inland of Totten Glacier (2 lakes), and inland of the Rutford (1 lake), Mercer (2 lakes), Whillans (3 lakes) and Kamb  
ice streams (1 lake) (Scambos et al., 2011; Wright and Siegfried, 2012; Siegfried and Fricker, 2018).

The location of our identified subglacial lakes demonstrate that thicker, fast-flowing upstream ice is not a pre-requisite for  
375 active subglacial lake existence at least in this part of East Antarctica. All seven lakes are located below sea level and below  
ice thicknesses of 812-1524 m (Table 1; Fig. 1b). In contrast, the mean ice thickness of previously-reported active lakes in  
Antarctica is 2272 m (Livingstone et al., 2022). The new lakes are generally located beneath slow-flowing ice (<65 m a<sup>-1</sup>) (Fig.  
1b). This contrasts with most known active lakes within 100 km of the Antarctic grounding line that lie beneath fast-flowing  
ice (>200 m a<sup>-1</sup>; Gardner et al., 2018; Livingstone et al., 2022). Two exceptions are Lakes KT2 (31.7 km<sup>2</sup>) and KT3 (38.7 km<sup>2</sup>)  
380 beneath the Kamb Ice Stream, which are comparable in area to our Lakes L1 and R1 (31-38 km<sup>2</sup>) and are located under near-  
stagnant ice (<2 m a<sup>-1</sup>) (Kim et al., 2016; Siegfried and Fricker, 2018). Another exception is the active lake system beneath  
Haynes Glacier in West Antarctica, where ice flow speed is ~131 m a<sup>-1</sup> (Hoffman et al., 2020). Ice thickness above these three  
lakes (820 – 1845 m) is within a similar range to our lakes (828-1503 m, Table 1). Much of the grounded ice along the Antarctic  
ice margin is slow-flowing (<200 m a<sup>-1</sup>) and lies below sea level within a similar ice thickness range. Consequently,  
385 moderately-sized near-margin active subglacial lakes similar to the ones presented here at 1-10 km in length and at least 20 –



40 km<sup>2</sup> are likely under-represented in Antarctic-wide inventories, yet could store and release significant volumes of water. Large volumes of water stored and released by these subglacial lakes could regulate downstream ice flow (Siegfried et al., 2016) and control ice margin water outlet locations, driving sub-ice shelf circulation and melting that could impact ice-shelf stability (e.g. Jenkins et al., 2011, Gwyther et al., 2023).

390

That these lakes are located so close to the ice margin beneath relatively slowly-flowing ice is unexpected, since thick ice and low surface mass balance at inland regions of Antarctica are typically associated with thawing ice-sheet bed where geothermal heat flow and ice flow speeds are low (Pattyn et al., 2016). However, the presence of these lakes in coastal DML indicates that there are temperate basal conditions where meltwater is accumulating either in situ or is sourced from pressure changes upstream that trigger drainage further downstream along a channelized subglacial system (Hoffman et al., 2020; Neckel et al., 2021; Dow et al., 2022). The ensemble analyses of bed topographies indicate that the detected lakes have large potential upstream catchments, ranging from  $0.5 \times 10^4$  km<sup>2</sup> (R1) to  $2.3 \times 10^4$  km<sup>2</sup> (V1; Table 1). For lakes located beneath slow-flowing ice, upstream subglacial meltwater supply is primarily controlled by geothermal heat flow (Malczyk et al., 2020) and model results suggest grounded basal ice across DML is at the pressure melting point (Pattyn, 2010). Therefore, lake recharge is likely regulated by geothermal heat flow, not by frictional heat generated by fast-flowing ice streams or outlet glaciers. The spatial distribution of our lakes can be used to constrain estimates of geothermal heat flow by calculating the minimum geothermal heat flow needed to keep the ice-sheet base at pressure melting point at the lake locations (Wright et al., 2012). Given that our estimated lake recharge rate for Lake R1 is  $0.03 \text{ km}^3 \text{ a}^{-1}$  and the subglacial drainage catchment is  $0.5 \times 10^4 \text{ km}^2$ , the mean basal melt rate required over the basin to fill Lake R1 can be approximated as  $0.03 \text{ km}^3 \text{ a}^{-1} / 0.5 \times 10^4 \text{ km}^2 = 6 \text{ mm a}^{-1}$ . Similarly, for Lake L1 the required basal melt rate can be approximated as  $2.2 \text{ mm a}^{-1}$ . This is within a reasonable range for coastal DML, where ice sheet model experiments have suggested that the mean basal melt rate can reach up to  $10 \text{ mm a}^{-1}$  beneath grounded ice (Pattyn, 2010).

None of the new lakes in this study are beneath ice experiencing extensive surface meltwater production or ponding (Arthur et al., 2022; Mahagaonkar and Moholdt, 2022), meaning surface meltwater reaching the ice bed can be discounted as a potential influence on subglacial lake recharge/behaviour. However, a  $\sim 1.8$  km-wide surface elevation anomaly 5 km inland of the Nivlisen Ice Shelf grounding line was discounted as subglacial in origin because large volumes of supraglacial meltwater are known to pond and flow onto the ice shelf in this region (Dell et al., 2020; Arthur et al., 2022). Extensive supraglacial lake activity can produce large local apparent elevation change that can be misclassified as subglacial lake activity, although it is possible for subglacial lake drainage to create an ice-surface depression that provides a natural basin for surface meltwater to pond (Fan et al., 2023). Additionally, perennial buried lake drainage close to the grounding line can also produce surface elevation change signatures on the order of several metres. Approximately 40 km west of Lake R1, Dunmire et al. (2020) detected an average ice surface lowering of  $\sim 2.5$  m over 1 year and 8 months due to a buried lake draining, and Sentinel-1 data



420 indicated that the lake drained again three years later. In contrast, our results show that ice surface uplift and lowering over the seven subglacial lakes occurs over multi-year timescales, with a longer cyclicality (~2-5 years).

One possible consideration for the two lakes closest to the grounding line (<16 km, M1 and M2) is that the observed elevation anomalies along these four ICESat-2 tracks reflect seawater intrusion in the ice-shelf grounding zone. Tidal migrations of seawater intrusions up to 20 cm thick along subglacial troughs over timescales of several weeks have been reported from 425 Sentinel-1 differential InSAR up to 15 km upstream of the Amery Ice Shelf grounding line (Chen et al., 2023). Robel et al. (2022) also showed with numerical modelling that seawater intrusion over impermeable beds may occur up to tens of kilometres upstream of grounding lines. However, the magnitude of observed elevation anomalies at M1 and M2 (>2 m ice surface uplift) and the multi-year timescale of these changes indicates lake filling rather than intrusion of a centimetre-scale seawater sheet.

#### 430 **4.2 Lake filling and draining patterns**

We show that the seven lakes fill and drain over periods of several years (Fig. 3, Fig. 5). This is consistent with observations from ICESat and ICESat-2 measurements elsewhere in Antarctica, where lakes continuously drain or fill over 3 or 4 years (e.g. Fricker and Scambos, 2009; Fricker et al., 2007; Smith et al., 2009). Similarly, Livingstone et al. (2022) reported lakes in Antarctica exhibiting extended multi-year periods of quiescence (filling) and draining, based on the ratio of filling (ice surface 435 uplift) and draining (ice surface subsidence) of known active lakes.

The limited spatial coverage, observational frequency and duration of ICESat, ICESat-2 and REMA make it challenging to determine the frequency of lake fill-drain cycles and to resolve potential rapid, episodic lake drainages on daily to monthly timescales. There might also be some undetected smaller lakes as ICESat-2 repeat track spacing is up to 9 km in coastal DML, 440 while the smallest lakes we recorded were 5 km wide. Smaller, centimetre-scale surface expressions of lake activity or seawater intrusion on shorter timescales require more detailed or sensitive data like InSAR (Neckel et al., 2021). For example, Neckel et al. (2021) showed that eight lakes of comparable size (7-51 km<sup>2</sup>) inland of the Jutulstraumen Glacier drained in a cascade over 12 days to ~5 months. Consequently, the short-term dynamics and hydrological networks of the new lakes we report may be under sampled, as they could also form interconnected, cascading systems.

#### 445 **4.3 Subglacial water flow**

The agreement between our subglacial lake locations, predicted subglacial drainage pathways and ice-shelf channels indicates that these lakes are actively discharging subglacial meltwater through a channelized subglacial conduit system in coastal DML, likely routing subglacial water directly into ice-shelf cavities. Previously, this link was made for active lakes beneath fast-flowing ice streams e.g. beneath the MacAyeal Ice Stream and Thwaites Glacier in West Antarctica (Fricker et al., 2010, Smith 450 et al., 2017). Further work should compare simultaneous observations of ice surface height anomalies and ice velocity changes





to constrain how the subglacial hydrological system co-evolves with subglacial lake fill-drain activity and to determine the influence on ice-shelf dynamics in coastal DML. Similar investigations have been conducted for a series of subglacial drainage events along the Northeast Greenland Ice Stream using Sentinel-1 DInSAR (Andersen et al., 2023) and Thwaites Glacier using Sentinel-1 and GNSS (Hoffman et al., 2020).

455

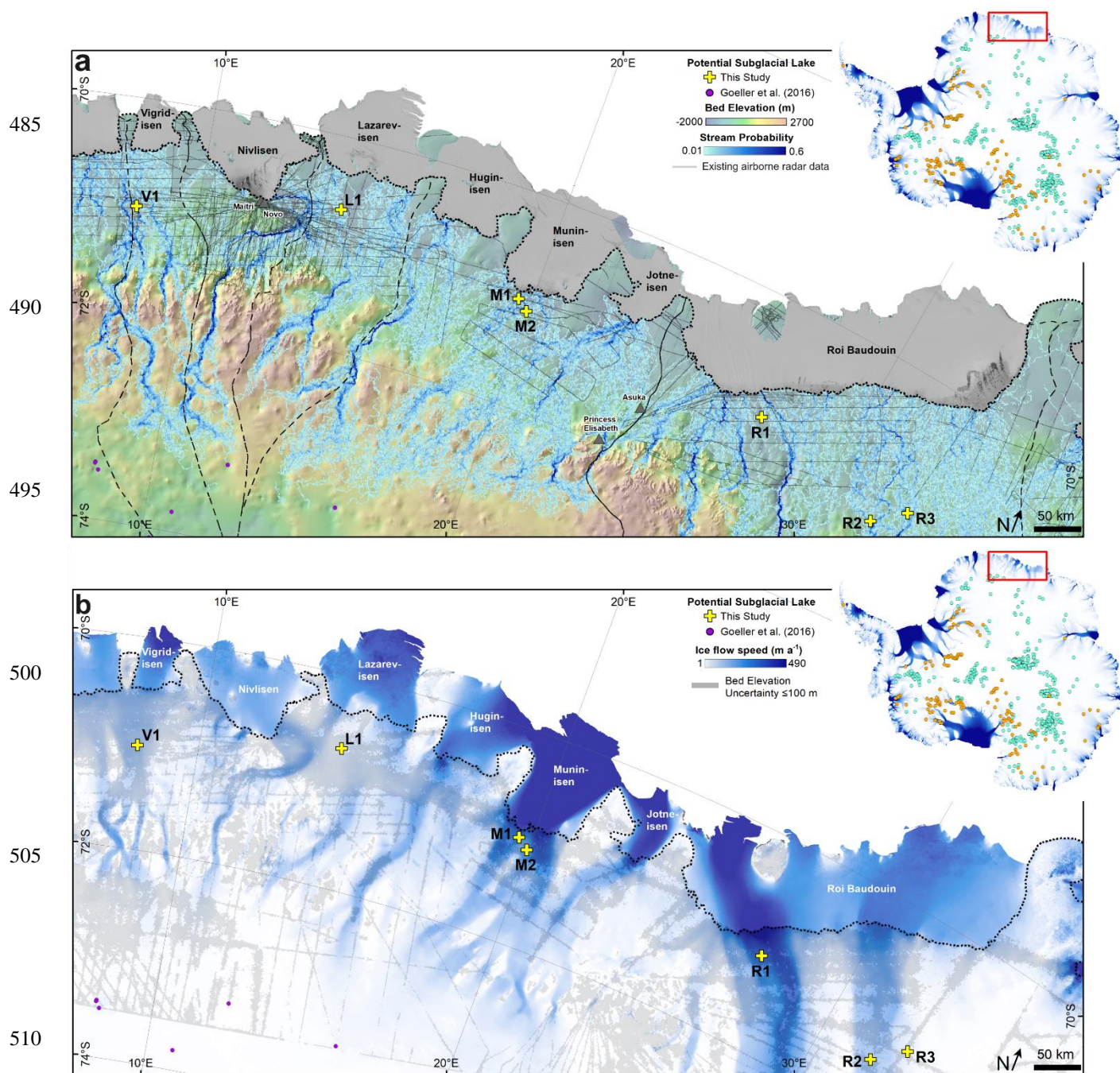
Our probability analysis of subglacial water routing shows increased uncertainty in drainage pathways downstream of Lakes V1, L1, R1 and R2 (Fig. 6c-f), mainly due to sparse radar survey coverage in these regions. Also, subglacial channels in these regions could also be ephemeral and only form during lake drainage events (Smith et al., 2017), and without strong topographic drivers of water flow it is possible that the routing of meltwater and outlet locations could be variable between events which could affect the location of subglacial meltwater outlets and consequently local sub-ice-shelf circulation and melt rates. Our analysis highlights regions where more densely-spaced radar profiles are needed to reduce uncertainty in basal topography and water routing, for example inland of the Roi Baudouin Ice Shelf and Lazarev Ice Shelf grounding lines. International coordinated programmes like RINGS (Matsuoka et al., 2022; [scar.org/science/cross/rings](https://scar.org/science/cross/rings)) involving new radar data collection along and inland of the Antarctic grounding line should help to close this knowledge gap.

460

## 465 **5 Summary and Outlook**

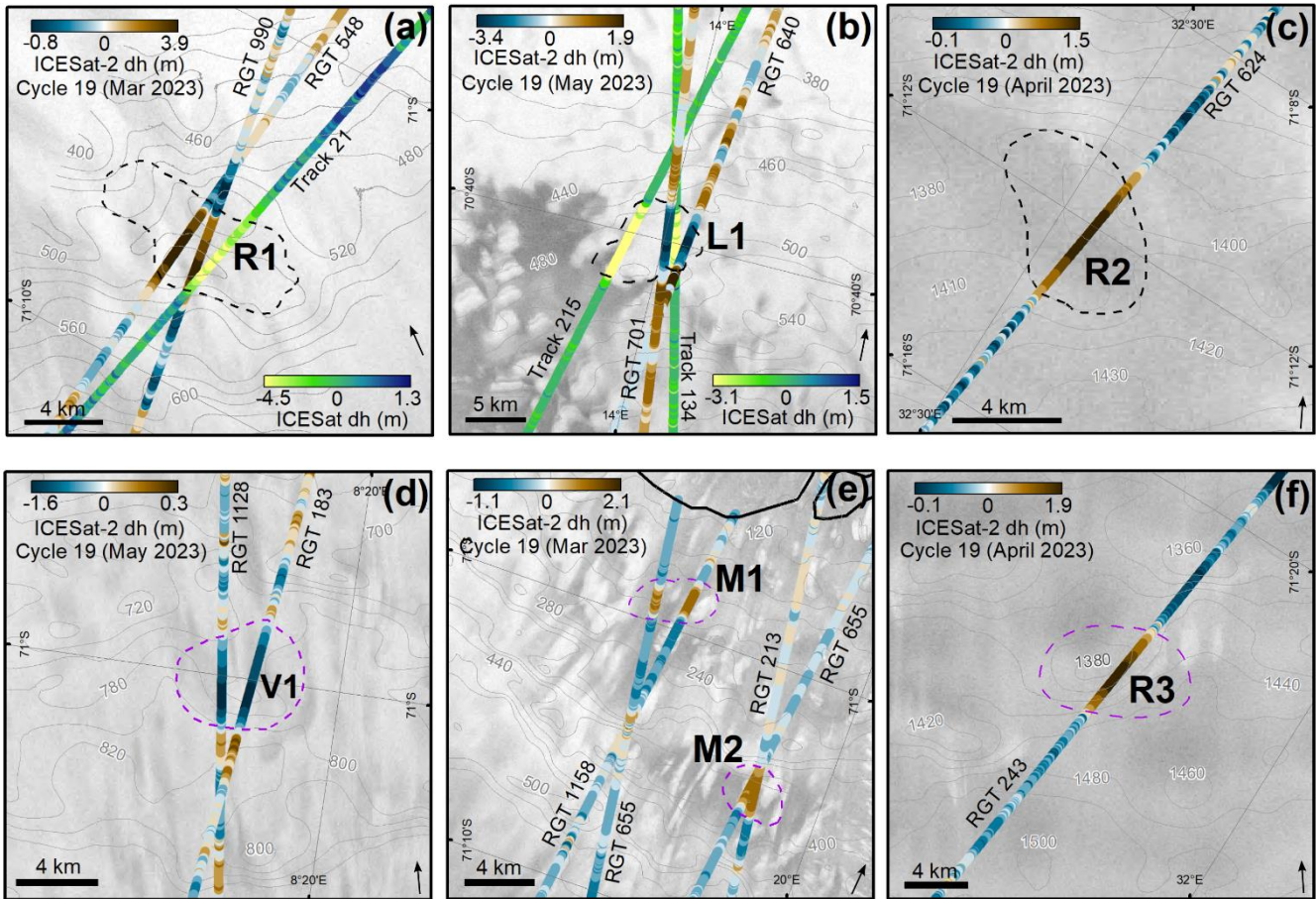
We identified seven local surface height anomalies of magnitudes up to  $\pm 4$  m using repeated ICESat-2 records in coastal DML, which we interpret as active subglacial lakes. The largest of these lakes was  $\sim 9$  km long and  $\sim 5$  km wide. ICESat laser altimetry and REMA strip differencing were used to extend the elevation change time series over three of these lakes. We detected multiple long-term lake fill-drain cycles from ICESat and ICESat-2 repeat tracks, which coincide spatially with elevation anomalies from differenced REMA strips. Six of the seven lakes coincide with predicted subglacial drainage systems using an ensemble of stochastically-simulated bed topographies that consider potential bed roughness between survey profiles. The combination of these datasets indicates that the hydrologically-active lakes fill and drain over several years and are linked to channelized subglacial drainage routing meltwater towards the grounding line in coastal DML. In contrast to previously detected subglacial lakes that are typically located under fast-flowing or thicker inland ice, the new lakes are found beneath slower-flowing ( $17\text{-}172\text{ m a}^{-1}$ ) grounded ice near the ice margin, with implications for ice dynamics and freshwater discharge beneath ice shelves. Our results improve knowledge of subglacial meltwater dynamics in this region of East Antarctica and provide new observational data to refine subglacial hydrological models, for example for validating predicted lake and stream locations. This refinement is crucial to accurately capture the complexity of dynamic basal conditions and their impact on to ice-sheet dynamics.

480



515 **Figure 1: The coastal region in Dronning Maud Land. (a) The locations of active subglacial lakes identified in this study in relation to predicted subglacial stream locations based on water routing analysis, bed topography and regional radar data availability. The dashed line is the MEASUREs grounding line (Rignot et al., 2016), bed elevations are from BedMachine (Morlighem et al., 2022), radar data availability is from Frémand et al. (2023), and the ice drainage divides (dashed lines) are from Mouginot et al. (2017). Subglacial lake locations in the inset map are from Livingstone et al. (2022), where active lakes are represented by orange dots and stable lakes by green dots. (b) Ice flow speed (Gardner et al., 2018) in blue shading and areas with bed elevation uncertainty <100 m based on the median absolute deviation between 50 bed topography simulations in this study (all other regions ≥100 m).**



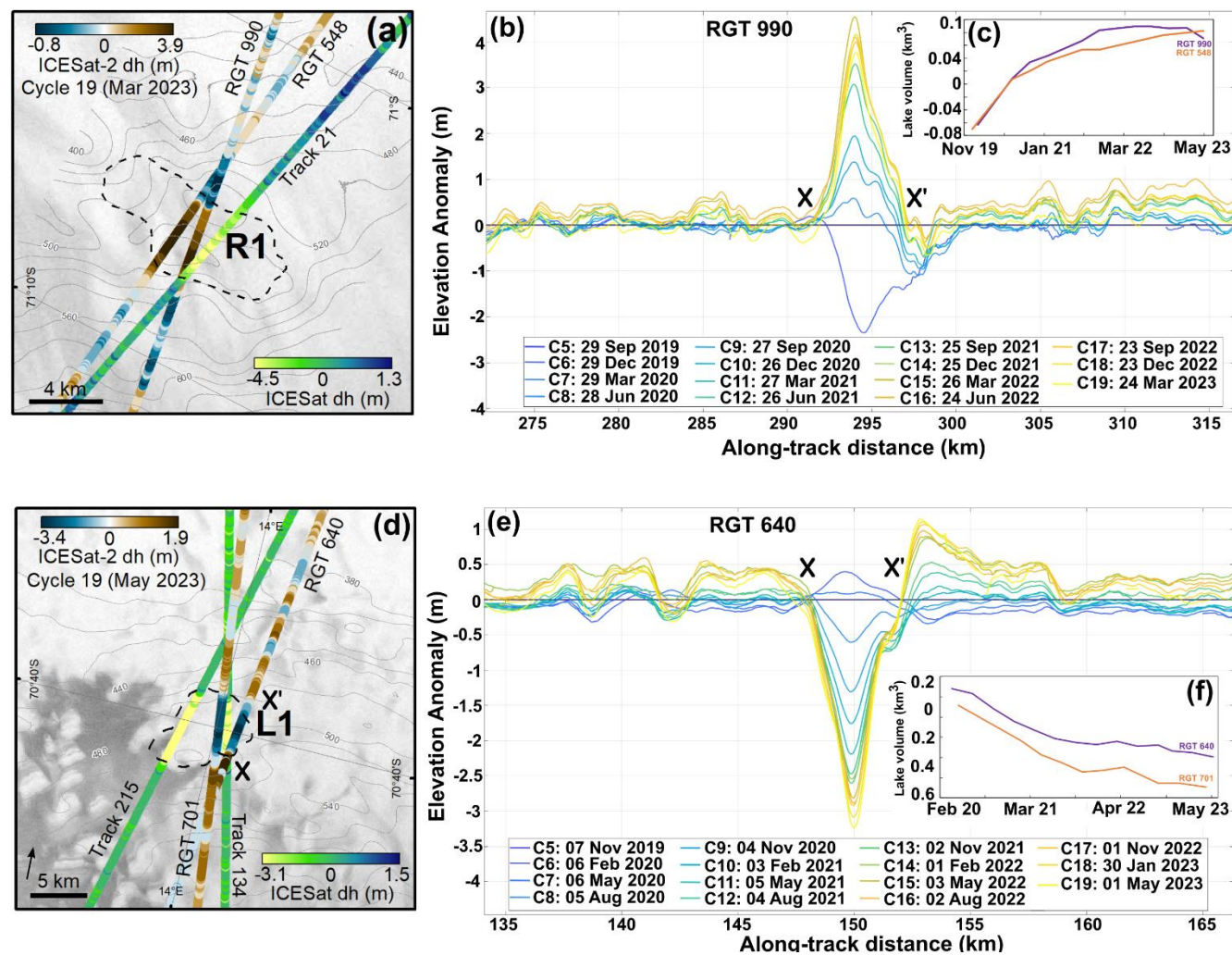


520

**Figure 2: Along-track surface elevation anomalies for each detected subglacial lake, indicating ice surface subsidence (subglacial lake draining) or uplift (subglacial lake filling). ICESat-2 tracks shown in Panels a-f and ICESat tracks shown in Panels a and b. Inferred lake boundaries derived from REMA differencing (Panels a, b and c; black dashed lines) or manual delineation (Panels d, e, f; purple dashed lines) are shown as dashed black outlines. Ice flow direction represented by black arrows (Gardner et al., 2018). Contours represent surface elevation from REMA (Howat et al., 2019). The bold black line in Panel (e) is the MEASUREs grounding line (Rignot et al., 2016). Other observed ice surface elevation changes do not meet the > 1 m anomaly criteria for active lakes (Section 2.5). Background image is the RADARSAT mosaic (Jezek et al., 2013).**

525

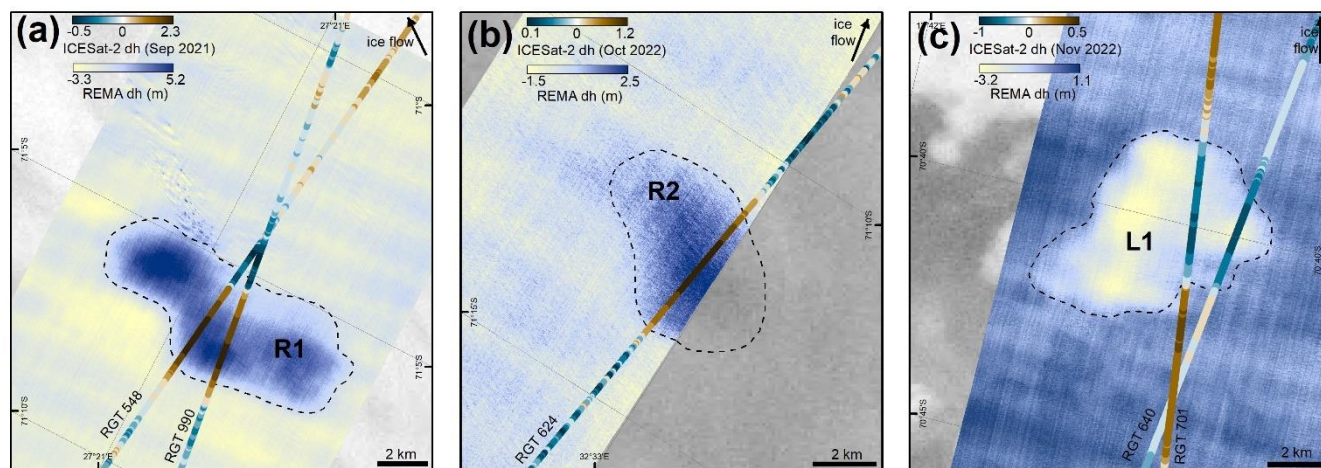
530



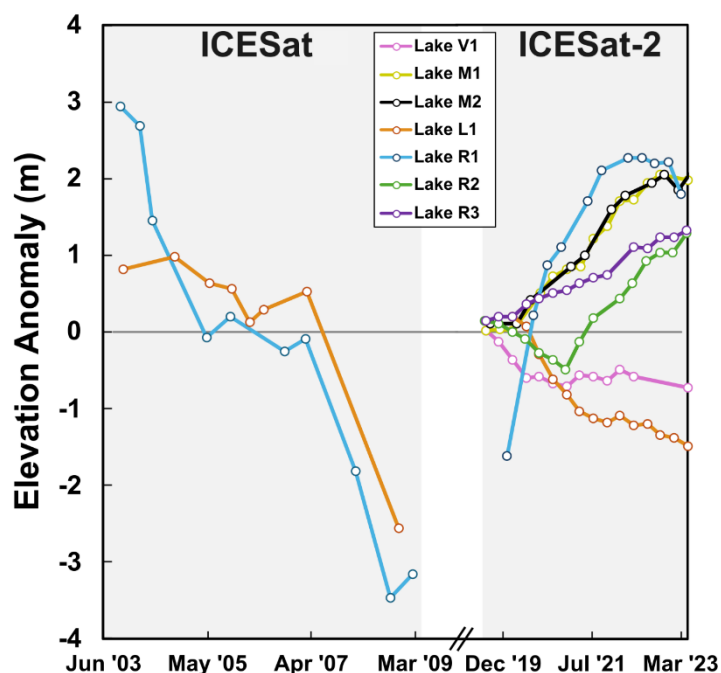
535 **Figure 3:** Ice surface elevation displacements for an actively filling lake (Lake R1, a-c) upstream of the Roi Baudouin Ice Shelf and  
 an actively draining lake (Lake L1, c-e) upstream of the Lazarev Ice Shelf, both derived from ICESat-2 and ICESat. Significant (>1  
 m) ice surface elevation anomalies along ICESat-2 tracks are highlighted by X-X' in each panel. Panels (b) and (e) show ice surface  
 elevation displacements relative to ICESat-2 Cycle 3 (April/May 2019). Colours correspond to each individual ICESat-2 cycle. Panels  
 (c) and (f) show time series of estimated lake volume.

540

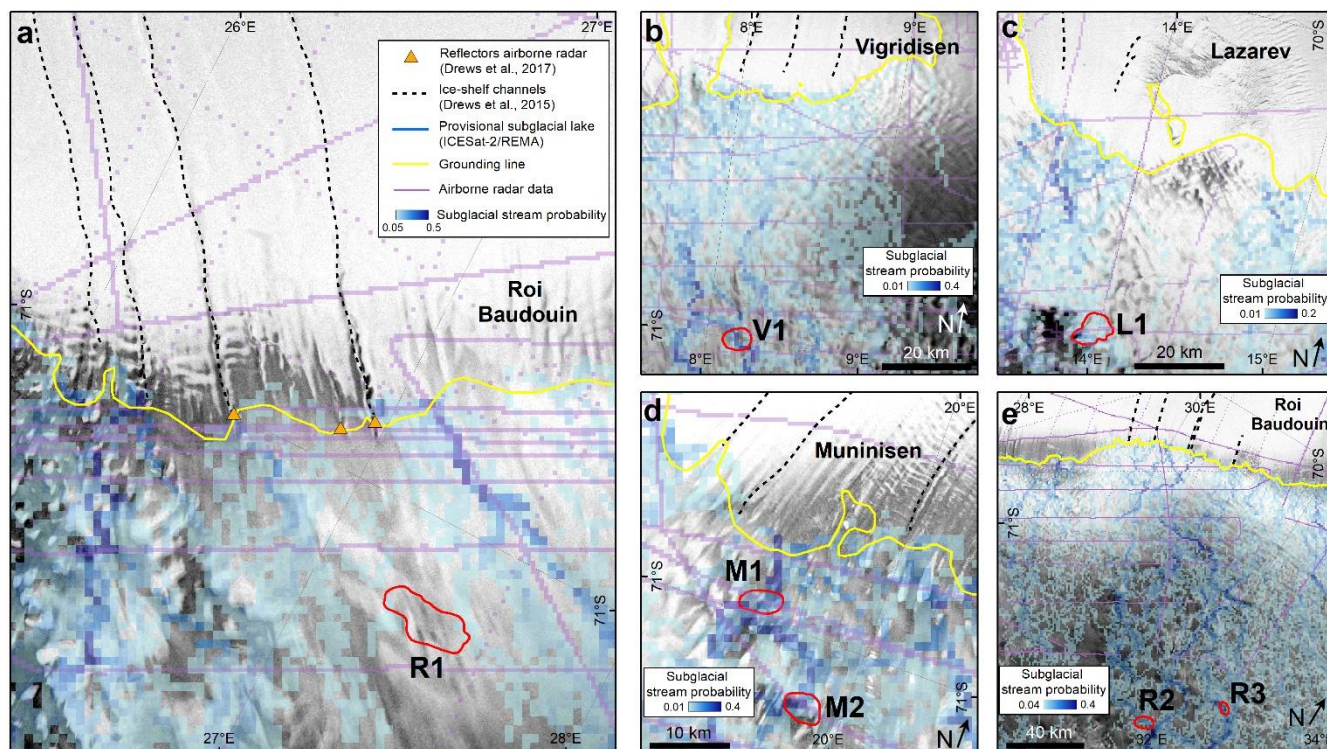




545 **Figure 4: Ice surface elevation change from REMA strip differencing. (a) Lake R1, and (b) Lake R2, both upstream of the Roi**  
**Baudouin Ice Shelf. (c) Lake L1 upstream of the Lazarev Ice Shelf. ICESat-2 elevation changes are relative to April 2019 (a) and**  
**May 2019 (b, c). Regions of localised elevation anomaly (blue shading for uplift and yellow shading for subsidence) between REMA**  
**strip pairs (22<sup>nd</sup> October 2019 – 10<sup>th</sup> January 2021 in Panel a, 18<sup>th</sup> January 2021 – 28<sup>th</sup> December 2022 in Panel b,**  
**25<sup>th</sup> January 2020 – 15<sup>th</sup> February 2021 in Panel c) are delineated by the dashed lines. These boundaries were outlined manually based on visual**  
 550 **assessment. Each example highlights the spatial co-occurrence between significant localised ice surface uplift/subsidence and surface**  
**elevation anomalies along the intersecting ICESat-2 tracks. The slight offset between the localised elevation anomalies in the ICESat-**  
**2 tracks and the REMA difference map over Lake R1 in Panel (a) could be due to lake boundary migration since the date of the**  
**REMA strip (January 2021).**



555 **Figure 5: ICESat and ICESat-2-derived ice surface elevation time series (calculated as median elevation anomalies within each lake**  
**boundary with respect to elevations in the first available cycle). Lakes L1, R1 and R2 use lake boundaries derived from REMA**  
 560 **differencing and Lakes V1, M1, M2 and R3 use boundaries based on locations of significant (>1 m) elevation anomalies over a**  
**distance of a kilometre or more.**  
 565



575

**Figure 6:** Simulated subglacial water routing and mapped ice-shelf channels in the vicinity of identified active lake areas in this study (red outlines). Ice-shelf channels (black dashed lines) are from Drews et al. (2015) (a-b) and manually delineated from REMA and RADARSAT imagery in this study (c-e). The yellow line is the MEaSUREs grounding line (Rignot et al., 2016), the purple lines are radar data locations from Frémand et al. (2023), and the orange triangles are reflectors in airborne radar data interpreted as subglacial water flow outlets (Drews et al., 2017). The background image is the RADARSAT mosaic (Jezek et al., 2013).

580





585 **Table 1: Subglacial lakes identified in this study. Lake areas are listed for those lakes where elevation anomalies were also derived from REMA strip differencing. Ice flow speed (Gardner et al., 2018), ice thickness (Fretwell et al., 2013; Morlighem et al., 2022) and bed elevation (Morlighem et al., 2022) are mean values within each inferred lake boundary. Bed elevation uncertainty is the median absolute deviation of 50 stochastic bed elevation simulations. Upstream catchment areas are mean values from the same topographic simulations.**

Lake Name	Location/Distance from Grounding Line	Centre Lon, Lat (decimal degrees)	Area (km <sup>2</sup> )	Ice flow speed (m a <sup>-1</sup> )	Bedmap2 ice thickness (m)	BedMachine ice thickness (m)	Upstream catchment area (km <sup>2</sup> )	Bed elevation (m above sea level)	Bed elevation uncertainty (m)
V1	Vigridisen (54 km)	8.19E, 70.99S	Unconfirmed	60	1247	1321	2.3 x 10 <sup>4</sup>	-552	58
L1	Lazarev (32 km)	13.97E, 70.67S	40.1	19	1020	1019	0.9 x 10 <sup>4</sup>	-558	47
M1	Muninisen (5 km)	19.60E, 70.98S	Unconfirmed	152	828	881	0.8 x 10 <sup>4</sup>	-724	28
M2	Muninisen (15 km)	19.87E, 71.07S	Unconfirmed	86	1008	924	1.2 x 10 <sup>4</sup>	-633	49
R1	Roi Baudouin (19 km)	27.41E, 71.10S	39.4	172	1137	1193	0.5 x 10 <sup>4</sup>	-737	76
R2	Roi Baudouin (115 km)	32.53E, 71.19S	21.5	17	1283	1391	1.4 x 10 <sup>4</sup>	-29	86
R3	Roi Baudouin (136 km)	31.65E, 71.44S	Unconfirmed	64	1503	1547	1.3x10 <sup>4</sup>	-162	97

590

### Data Availability

ICESat-2 ATL11 Level 3B version 6 land ice height data are freely available from <https://nsidc.org/data/atl11/versions/6>. ICESat GLA12 version 34 land ice height data are freely available from <https://nsidc.org/data/glah12/versions/34>. Ice surface velocities from ITS-LIVE (Gardner et al., 2019) are available at <https://its-live.jpl.nasa.gov/#data-portal>. The REMA ice surface DEM strips (Howat et al., 2019) are available from the U.S. Polar Geospatial Center at <https://www.pgc.umn.edu/data/rema/>. The delineated lake boundaries are available as a shapefile from the Norwegian Polar Data Centre via <https://doi.org/10.21334/npolar.2024.ab777130> and the predicted subglacial stream locations produced by our water routing analysis are available as a GeoTIFF from the Norwegian Polar Data Centre via <https://data.npolar.no/dataset/10.21334/npolar.2024.b438191c>.

595



## 600 Code Availability

Code used to process and plot ICESat-2 ATL11 Level 3B version 6 land ice height data and ICESat GLAH12 version 34 land ice height data are available at [https://github.com/JennyFArthur/DML\\_SubglacialLakes](https://github.com/JennyFArthur/DML_SubglacialLakes).

## Author Contributions

605 JA analysed the ICESat-2 and REMA data, performed the identification of active lakes, analysed the results and wrote the paper with input from all co-authors. CS and KM carried out stochastic bed topography simulations and the subglacial water flow routing analysis. GM contributed to the conception of the study and processed the ICESat data. All authors contributed to the discussion of the results and to editing of the manuscript.

## Competing Interests

The contact author has declared that none of the authors have any competing interests.

## 610 Acknowledgements

JA and CS are funded by the Research Council of Norway's FRINATEK project (project number: 315246). JA is also funded by a national infrastructure grant from the Norwegian Space Agency to the Norwegian Polar Institute (contract number: 74CO2303). The bed elevation simulations were performed on resources provided by Sigma2 - the National Infrastructure for High-Performance Computing and Data Storage in Norway through project NN10061K.

## 615 References

- Andersen, J.K., Rathmann, N., Hvidberg, C.S., Grinsted, A., Kusk, A., Merryman Boncori, J.P. and Mouginot, J.: Episodic subglacial drainage cascades below the Northeast Greenland Ice Stream. *Geophys. Res. Lett.*, 50(12), <https://doi.org/10.1029/2023GL103240>, 2023.
- 620 Arthur, J.F., Stokes, C.R., Jamieson, S.S., Rachel Carr, J., Leeson, A.A. and Verjans, V.: Large interannual variability in supraglacial lakes around East Antarctica. *Nat. Commun.*, 13(1), 1711, <https://doi.org/10.1038/s41467-022-29385-3>, 2022.
- Boening, C., Lebsack, M., Landerer, F. and Stephens, G.: Snowfall-driven mass change on the East Antarctic Ice Sheet. *Geophys. Res. Lett.*, 39(21), <https://doi.org/10.1029/2012GL053316>, 2012.
- Brenner, A.C., DiMarzio, J.P. and Zwally, H.J.: Precision and accuracy of satellite radar and laser altimeter data over the continental ice sheets. *IEEE Trans. Geosci. Remote Sens.*, 45(2), 321-331, <https://doi.org/10.1109/TGRS.2006.887172> 2007.
- 625 Brunt, K.M., Smith, B.E., Sutterley, T.C., Kurtz, N.T., Neumann, T.A.: Comparisons of Satellite and Airborne Altimetry With Ground-Based Data From the Interior of the Antarctic Ice Sheet. *Geophys. Res. Lett.*, 48(2), e2020GL090572, <https://doi.org/10.1029/2020GL090572>, 2020.



- 630 Carter, S.P. and Fricker, H.A.: The supply of subglacial meltwater to the grounding line of the Siple Coast, West Antarctica. *Ann. Glaciol.*, 53(60), 267-280, <https://doi.org/10.3189/2012AoG60A119>, 2012.
- Carter, S.P., Fricker, H.A., Blankenship, D.D., Johnson, J.V., Lipscomb, W.H., Price, S.F. and Young, D.A.: Modeling 5 years of subglacial lake activity in the MacAyeal Ice Stream (Antarctica) catchment through assimilation of ICESat laser altimetry. *J. Glaciol.*, 57(206), 1098-1112, <https://doi.org/10.3189/002214311798843421>, 2011.
- 635 Chartrand, A.M. and Howat, I.M.: Basal channel evolution on the Getz Ice Shelf, West Antarctica. *J. Geophys. Res.*, 125(9), <https://doi.org/10.1029/2019JF005293>, 2020.
- Chen, H., Rignot, E., Scheuchl, B. and Ehrenfeucht, S.: Grounding zone of Amery Ice Shelf, Antarctica, from differential synthetic-aperture radar interferometry. *Geophys. Res. Lett.*, 50(6), <https://doi.org/10.1029/2022GL102430>, 2023.
- Davison, B.J., Hogg, A.E., Gourmelen, N., Jakob, L., Wuite, J., Nagler, T., Greene, C., Andreasen, J., Engdahl, M.: Annual mass budget of Antarctic ice shelves from 1997 to 2021. *Sci. Adv.* 9, <https://doi.org/10.1126/sciadv.adi0186>, 2023.
- 640 Dell, R., Arnold, N., Willis, I., Banwell, A., Williamson, A., Pritchard, H. and Orr, A.: Lateral meltwater transfer across an Antarctic ice shelf. *The Cryosphere*, 14(7), 2313-2330, <https://doi.org/10.5194/tc-14-2313-2020>, 2020.
- Dow, C.F., Ross, N., Jeofry, H., Siu, K. and Siegert, M.J.: Antarctic basal environment shaped by high-pressure flow through a subglacial river system. *Nat. Geosci.*, 15(11), 892-898, <https://doi.org/10.1038/s41561-022-01059-1>, 2022.
- 645 Drews, R.: Evolution of ice-shelf channels in Antarctic ice shelves. *The Cryosphere*, 9, 1169–1181, <https://doi.org/10.5194/tc-9-1169-2015>, 2015.
- Drews, R., Pattyn, F., Hewitt, I.J., Ng, F.S.L., Berger, S., Matsuoka, K., Helm, V., Bergeot, N., Favier, L. and Neckel, N.: Actively evolving subglacial conduits and eskers initiate ice shelf channels at an Antarctic grounding line. *Nat. Commun.*, 8(1), 15228, <https://doi.org/10.1038/ncomms15228>, 2017.
- 650 Drews, R., Schannwell, C., Ehlers, T.A., Gladstone, R., Pattyn, F. and Matsuoka, K.: Atmospheric and oceanographic signatures in the ice shelf channel morphology of Roi Baudouin Ice Shelf, East Antarctica, inferred from radar data. *J. Geophys. Res.*, 125(7), <https://doi.org/10.1029/2020JF005587>, 2020.
- Dunmire, D., Lenaerts, J.T.M., Banwell, A.F., Wever, N., Shragge, J., Lhermitte, S., Drews, R., Pattyn, F., Hansen, J.S.S., Willis, I.C. and Miller, J.: Observations of buried lake drainage on the Antarctic Ice Sheet. *Geophys. Res. Lett.*, 47(15), <https://doi.org/10.1029/2020GL087970>, 2020.
- 655 ESA.: Sentinel-1: ESA's Radar Observatory Mission for GMES Operational Services. ESA SP-1322/1, ISBN 978-92-9221-418-0, 2012.
- Fan, Y.; Hao, W.; Zhang, B.; Ma, C.; Gao, S.; Shen, X.; Li, F.: Monitoring the Hydrological Activities of Antarctic Subglacial Lakes Using CryoSat-2 and ICESat-2 Altimetry Data. *Remote Sens.* 14, 898, <https://doi.org/10.3390/rs14040898>, 2022.
- 660 Fan, Y., Ke, C.Q., Shen, X., Xiao, Y., Livingstone, S.J. and Sole, A.J.: Subglacial lake activity beneath the ablation zone of the Greenland Ice Sheet. *The Cryosphere*, 17(4), 1775-1786, <https://doi.org/10.5194/tc-17-1775-2023>, 2023.



- Flament, T., Berthier, E. and Rémy, F.: Cascading water underneath Wilkes Land, East Antarctic ice sheet, observed using altimetry and digital elevation models. *The Cryosphere*, 8(2), 673–687, <https://doi.org/10.5194/tc-8-673-2014>, 2014.
- 665 Frémand, A.C., Fretwell, P., Bodart, J.A., Pritchard, H.D., Aitken, A., Bamber, J.L., Bell, R., Bianchi, C., Bingham, R.G., Blankenship, D.D. and Casassa, G.: Antarctic Bedmap data: Findable, Accessible, Interoperable, and Reusable (FAIR) sharing of 60 years of ice bed, surface, and thickness data. *Earth Syst. Sci. Data*, 15(7), <https://doi.org/10.5194/essd-15-2695-2023>, 2023.
- Fricker, H.A., Scambos, T., Bindschadler, R., and Padman, L.: An Active Subglacial Water System in West Antarctica Mapped from Space. *Science*, 315(5818): 1544–1548, <https://doi.org/10.1126/science.1136897>, 2007.
- 670 Fricker, H.A. and Scambos, T.: Connected subglacial lake activity on lower Mercer and Whillans ice streams, West Antarctica, 2003–2008. *J. Glaciol.*, 55(190), 303–315, <https://doi.org/10.3189/002214309788608813>, 2009.
- Fricker, H.A., Scambos, T., Carter, S., Davis, C., Haran, T. and Joughin, I.: Synthesizing multiple remote-sensing techniques for subglacial hydrologic mapping: application to a lake system beneath MacAyeal Ice Stream, West Antarctica. *J. Glaciol.*, 56(196), 187–199, <https://doi.org/10.3189/002214310791968557>, 2010.
- 675 Fricker HA, Carter SP, Bell RE, Scambos T.: Active lakes of Recovery Ice Stream, East Antarctica: a bedrock-controlled subglacial hydrological system. *J. Glaciol.*, 60(223), 1015–1030, <https://doi.org/10.3189/2014JoG14J063>, 2014.
- Gardner, A. S., G. Moholdt, T. Scambos, M. Fahnestock, S. Ligtenberg, M. van den Broeke, and J. Nilsson: Increased West Antarctic and unchanged East Antarctic ice discharge over the last 7 years, *The Cryosphere*, 12(2): 521–547, <https://doi.org/10.5194/tc-12-521-2018>, 2018.
- 680 Goeller, S., Steinhage, D., Thoma, M. and Grosfeld, K.: Assessing the subglacial lake coverage of Antarctica. *Ann. Glaciol.*, 57(72), 109–117, <https://doi.org/10.1017/aog.2016.23>, 2016.
- Goldberg, D., Twelves, A., Holland, P., Wearing, M.G.: The Non-Local Impacts of Antarctic Subglacial Runoff. *JGR Oceans* 128(10) <https://doi.org/10.1029/2023JC019823>, 2023.
- 685 Gong, F., Zhang, K. and Liu, S.: Retrieving the grounding lines of the Riiser-Larsen Ice Shelf using Sentinel-1 SAR images. *Int. J. Digit. Earth*, 16(1), 2467–2486, <https://doi.org/10.1080/17538947.2023.2229785>, 2023.
- Gray, L., Joughin, I., Tulaczyk, S., Spikes, V.B., Bindschadler, R. and Jezek, K.: Evidence for subglacial water transport in the West Antarctic Ice Sheet through three-dimensional satellite radar interferometry. *Geophys. Res. Lett.*, 32(3), <https://doi.org/10.1029/2004GL021387>, 2005.
- 690 Gwyther, D.E., Dow, C.F., Jendersie, S., Gourmelen, N. and Galton-Fenzi, B.K.: Subglacial freshwater drainage increases simulated basal melt of the Totten Ice Shelf. *Geophys. Res. Lett.*, 50(12), <https://doi.org/10.1029/2023GL103765>, 2023.
- Hayden, A., & Dow, C.: Examining the effect of ice dynamic changes on subglacial hydrology through modelling of a synthetic Antarctic glacier. *J. Glaciol.*, 1–14. <https://doi.org/10.1017/jog.2023.65>, 2023.



- 695 Hodgson, D.A., Jordan, T.A., Ross, N., Riley, T.R. and Fretwell, P.T.: Drainage and refill of an Antarctic Peninsula subglacial lake reveal an active subglacial hydrological network. *The Cryosphere*, 16(12), 4797-4809, <https://doi.org/10.5194/tc-16-4797-2022>, 2022.
- Hogg, A., Shepherd, A., Gourmelen, N., & Engdhal, M.: Grounding line migration from 1992 to 2011 on Petermann Glacier, North-West Greenland. *J. Glaciol.*, 62(236), 1104-1114, <https://doi.org/10.1017/jog.2016.83>, 2016.
- 700 Howat, I.M., Porter, C., Smith, B.E., Noh, M.J. and Morin, P.: The reference elevation model of Antarctica. *The Cryosphere*, 13(2), 665-674, <https://doi.org/10.5194/tc-13-665-2019>, 2019.
- Humbert, A., Steinhage, D., Helm, V., Beyer, S. and Kleiner, T.: Missing evidence of widespread subglacial lakes at Recovery Glacier, Antarctica. *J. Geophys. Res.*, 123(11), 2802-2826, <https://doi.org/10.1029/2017JF004591>, 2018.
- Jenkins, A.: Convection-driven melting near the grounding lines of ice shelves and tidewater glaciers. *JPO*, 41(12), 2279-2294, <https://doi.org/10.1175/JPO-D-11-03.1>, 2011.
- 705 Kim, B.H., Lee, C.K., Seo, K.W., Lee, W.S. and Scambos, T.: Active subglacial lakes and channelized water flow beneath the Kamb Ice Stream. *The Cryosphere*, 10(6), 2971-2980, <https://doi.org/10.5194/tc-10-2971-2016>, 2016.
- Kohler, J., Neumann, T.A., Robbins, J.W., Tronstad, S. and Melland, G.: ICESat elevations in Antarctica along the 2007–09 Norway–USA traverse: Validation with ground-based GPS. *IEEE GRSL*, 51(3), 1578-1587, <https://doi.org/10.1109/TGRS.2012.2207963>, 2012.
- 710 Le Brocq, A.M., Ross, N., Griggs, J.A., Bingham, R.G., Corr, H.F., Ferraccioli, F., Jenkins, A., Jordan, T.A., Payne, A.J., Rippin, D.M. and Siegert, M.J.: Evidence from ice shelves for channelized meltwater flow beneath the Antarctic Ice Sheet. *Nat. Geosci.*, 6(11), 945-948, <https://doi.org/10.1038/ngeo1977>, 2013.
- Lepp, A.P., Simkins, L.M., Anderson, J.B., Clark, R.W., Wellner, J.S., Hillenbrand, C.D., Smith, J.A., Lehrmann, A.A., Totten, R., Larter, R.D. and Hogan, K.A.: Sedimentary signatures of persistent subglacial meltwater drainage from Thwaites Glacier, Antarctica. *Front. Earth Sci.*, 10, <https://doi.org/10.3389/feart.2022.863200>, 2022.
- 715 Liang, D., Guo, H., Zhang, L., Li, H. and Wang, X.: Sentinel-1 EW mode dataset for Antarctica from 2014–2020 produced by the CASEarth Cloud Service Platform. *Big Earth Data*, 6(4), 385-400, <https://doi.org/10.1080/20964471.2021.1976706>, 2022.
- 720 Livingstone, S.J., Li, Y., Rutishauser, A., Sanderson, R.J., Winter, K., Mikucki, J.A., Björnsson, H., Bowling, J.S., Chu, W., Dow, C.F. and Fricker, H.A.: Subglacial lakes and their changing role in a warming climate. *Nat. Rev. Earth Environ.*, 3(2), 106-124, <https://doi.org/10.1038/s43017-021-00246-9>, 2022.
- MacKie, E. J., Field, M., Wang, L., Yin, Z., Schoedl, N., Hibbs, M., & Zhang, A.: GStatSim V1.0: A Python package for geostatistical interpolation and conditional simulation. *GMD*, 16(13), 3765–3783, <https://doi.org/10.5194/gmd-16-3765-2023>, 2023.
- 725 Mahagaonkar, A., Moholdt, G.: Surface meltwater lake extents and depths for 5 ice shelves of DML, East Antarctica, 2014-2021 [Data set]. Norwegian Polar Institute. <https://doi.org/10.21334/npolar.2023.31aae21f>, 2022.



- Malczyk, G., Gourmelen, N., Goldberg, D., Wuite, J. and Nagler, T.: Repeat subglacial lake drainage and filling beneath Thwaites Glacier. *Geophys. Res. Lett.*, 47(23), <https://doi.org/10.1029/2020GL089658>, 2020.
- 730 Malczyk G, Gourmelen N, Werder M, Wearing M, Goldberg D.: Constraints on subglacial melt fluxes from observations of active subglacial lake recharge. *J. Glaciol.*, 1-15, <https://doi.org/10.1017/jog.2023.70>, 2023.
- Markus, T., Neumann, T., Martino, A., Abdalati, W., Brunt, K., Csatho, B., Farrell, S., Fricker, H., Gardner, A., Harding, D. and Jasinski, M.: The Ice, Cloud, and land Elevation Satellite-2 (ICESat-2): science requirements, concept, and implementation. *Remote Sens. Environ.*, 190, 260-273, <https://doi.org/10.1016/j.rse.2016.12.029>, 2017.
- 735 Matsuoka, K., Forsberg, R., Ferraccioli, F., Moholdt, G., and Morlighem, M.: Circling Antarctica to unveil the bed below its icy edge, *Eos*, 103, <https://doi.org/10.1029/2022EO220276>, 2022.
- Medley, B., Lenaerts, J.T.M., Dattler, M., Keenan, E. and Wever, N.: Predicting Antarctic net snow accumulation at the kilometer scale and its impact on observed height changes. *Geophys. Res. Lett.*, 49(20), <https://doi.org/10.1029/2022GL099330>, 2022.
- 740 Miles, B.W., Stokes, C.R., Jamieson, S.S., Jordan, J.R., Gudmundsson, G.H. and Jenkins, A.: High spatial and temporal variability in Antarctic ice discharge linked to ice shelf buttressing and bed geometry. *Sci. Rep.*, 12(1), 10968, <https://doi.org/10.1038/s41598-022-13517-2>, 2022.
- Moholdt, G., Nuth, C., Hagen, J.O., Kohler, J.: Recent elevation changes of Svalbard glaciers derived from ICESat laser altimetry. *Remote Sens. Environ.* 114(11), 2756-2767, <https://doi.org/10.1016/j.rse.2010.06.008>, 2010.
- 745 Moon, J., Lee, H. and Lee, H.: Elevation Change of CookE2 Subglacial Lake in East Antarctica Observed by DInSAR and Time-Segmented PSInSAR. *Remote Sens.*, 14(18), 4616, <https://doi.org/10.3390/rs14184616>, 2022.
- Morlighem, M.: MEaSURES BedMachine Antarctica, Version 3 [Data Set]. Boulder, Colorado USA. NASA National Snow and Ice Data Center Distributed Active Archive Center. Date Accessed 11-22-2023, <https://doi.org/10.5067/FPSU0V1MWUB6>, 2022.
- 750 Mougnot, J., B. Scheuchl, and E. Rignot. 2017. MEASURE's Antarctic Boundaries for IPY 2007-2009 from Satellite Radar, Version 2. Boulder, Colorado USA. NASA National Snow and Ice Data Center Distributed Active Archive Center. doi: <http://dx.doi.org/10.5067/AXE4121732AD>.
- Neckel, N., Franke, S., Helm, V., Drews, R. and Jansen, D.; Evidence of Cascading Subglacial Water Flow at Jutulstraumen Glacier (Antarctica) Derived From Sentinel-1 and ICESat-2 Measurements. *Geophys. Res. Lett.*, 48(20), <https://doi.org/10.1029/2021GL094472>, 2021.
- 755 Nilsson, J., Gardner, A. S., and Paolo, F. S.: Elevation change of the Antarctic Ice Sheet: 1985 to 2020, *Earth Syst. Sci. Data*, 14, 3573–3598, <https://doi.org/10.3189/002214308784886171>, 2022.
- Pattyn, F.: Investigating the stability of subglacial lakes with a full Stokes ice-sheet model. *J. Glaciol.*, 54(185), 353-361, 2008.
- Pattyn, F.: Antarctic subglacial conditions inferred from a hybrid ice sheet/ice stream model. *EPSL* 295(3-4), 451-461, <https://doi.org/10.1016/j.epsl.2010.04.025>, 2010.
- 760





- Pattyn, F., Carter, S.P. and Thoma, M.: Advances in modelling subglacial lakes and their interaction with the Antarctic ice sheet. *Philos Trans A Math Phys Eng Sci*, 374(2059), <https://doi.org/10.1098/rsta.2014.0296>, 2016.
- Priergaard Zinck, A., Wouters, B., Lambert, E., Lhermitte, S.; Unveiling spatial variability within the Dotson Melt Channel through high-resolution basal melt rates from the Reference Elevation Model of Antarctica. *The Cryosphere* 17(9) 3785-3801, <https://doi.org/10.5194/tc-17-3785-2023>, 2023.
- 765 Rignot, E., Mouginot, J., and Scheuchl, B.: MEaSUREs Antarctic Grounding Line from Differential Satellite Radar Interferometry, Version 2. Boulder, Colorado USA. NASA National Snow and Ice Data Center Distributed Active Archive Center. <https://doi.org/10.5067/IKBWW4RYHF1Q>, 2016.
- Robel, A.A., Wilson, E. and Seroussi, H.: Layered seawater intrusion and melt under grounded ice. *The Cryosphere*, 16(2), 451-469, <https://doi.org/10.5194/tc-16-451-2022>, 2022.
- 770 Scambos, T.A, Berthier, E., Shuman, C.A.: The triggering of subglacial lake drainage during rapid glacier drawdown: Crane Glacier, Antarctic Peninsula. *Ann. Glaciol.* 52(59), 74-82, <https://doi.org/10.3189/172756411799096204>, 2011.
- Schodlok, M.P., Menemenlis, D. and Rignot, E.J.: Ice shelf basal melt rates around Antarctica from simulations and observations. *J. Geophys. Res. Oceans*, 121(2), 1085-1109, <https://doi.org/10.1002/2015JC011117>, 2016.
- 775 Sergienko, O.V., MacAyeal, D.R. and Bindschadler, R.A.: Causes of sudden, short-term changes in ice-stream surface elevation. *Geophys. Res. Lett.*, 34(22), <https://doi.org/10.1029/2007GL031775>, 2007.
- Shackleton, C., Matsuoka, K., Moholdt, G., Van Liefferinge, B. and Paden, J.: Stochastic simulations of bed topography constrain geothermal heat flow and subglacial drainage near Dome Fuji, East Antarctica. *J. Geophys. Res.*, 128(11), <https://doi.org/10.1029/2023JF007269>, 2023.
- 780 Shean, D.E., Joughin, I.R., Dutrieux, P., Smith, B.E. and Berthier, E.: Ice shelf basal melt rates from a high-resolution digital elevation model (DEM) record for Pine Island Glacier, Antarctica. *The Cryosphere*, 13(10), 2633-2656, <https://doi.org/10.5194/tc-13-2633-2019>, 2019.
- Shreve, R.L.: Movement of water in glaciers. *J. Glaciol.*, 11(62), 205-214, <https://doi.org/10.3189/S002214300002219X>, 1972.
- Siegfried, M., Fricker, H.A., Carter, S.P., Tulaczyk, T.: Episodic ice velocity fluctuations triggered by a subglacial flood in West Antarctica. *Geophys. Res. Lett.*, 43(6), 2640-2648, <https://doi.org/10.1002/2016GL067758>, 2016.
- 785 Siegfried, M.R. and Fricker, H.A.: Thirteen years of subglacial lake activity in Antarctica from multi-mission satellite altimetry. *Ann. Glaciol.*, 59(76pt1), 42-55, <https://doi.org/10.1017/aog.2017.36>, 2018.
- Siegfried, M.R. and Fricker, H.A.: Illuminating active subglacial lake processes with ICESat-2 laser altimetry. *Geophys. Res. Lett.*, 48(14), <https://doi.org/10.1029/2020GL091089>, 2021.
- 790 Smith, B.E., Fricker, H.A., Joughin, I.R., and Tulaczyk, S.: An inventory of active subglacial lakes in Antarctica detected by ICESat (2003-2008). *J. Glac.*, 2009. 55(192), 573-595, <https://doi.org/10.3189/002214309789470879>, 2009.
- Smith, B.E., Gourmelen, N., Huth, A. and Joughin, I.: Connected subglacial lake drainage beneath Thwaites glacier, west Antarctica. *The Cryosphere*, 11(1), 451-467, <https://doi.org/10.5194/tc-11-451-2017>, 2017.



- Smith, B., Fricker, H.A., Gardner, A.S., Medley, B., Nilsson, J., Paolo, F.S., Holschuh, N., Adusumilli, S., Brunt, K., Csatho, B. and Harbeck, K.: Pervasive ice sheet mass loss reflects competing ocean and atmosphere processes. *Science*, 368(6496), 1239-1242, <https://doi.org/10.1126/science.aaz5845>, 2020.
- Smith, B.E., Medley, B., Fettweis, X., Sutterley, T., Alexander, P., Porter, D. and Tedesco, M.: Evaluating Greenland surface-mass-balance and firn-densification data using ICESat-2 altimetry. *The Cryosphere*, 17(2), 789-808, <https://doi.org/10.5194/tc-17-789-2023>, 2023.
- 800 Stearns, L.A., Smith, B.E., and Hamilton, G.S.: Increased flow speed on a large East Antarctic outlet glacier caused by subglacial floods. *Nat. Geosci*, 2008. 1(12): 827-831, <https://doi.org/10.1038/ngeo356>, 2008.
- Tarboton, D.G.: A new method for the determination of flow directions and upslope areas in grid digital elevation models. *Water Resour. Res.*, 33(2), 309-319, <https://doi.org/10.1029/96WR03137>, 1997.
- Trusel, L.D., Frey, K.E., Das, S.B., Munneke, P.K. and Van Den Broeke, M.R.: Satellite-based estimates of Antarctic surface meltwater fluxes. *Geophys. Res. Lett.*, 40(23), 6148-6153, <https://doi.org/10.1002/2013GL058138>, 2013.
- Wadham, J.L., De'ath, R., Monteiro, F.M., Tranter, M., Ridgwell, A., Raiswell, R. and Tulaczyk, S.: The potential role of the Antarctic Ice Sheet in global biogeochemical cycles. *Earth Environ. Sci. Trans.*, 104(1), 55-67, <https://doi.org/10.1017/S1755691013000108>, 2013.
- Whiteford, A., Horgan, H.J., Leong, W.J. and Forbes, M.: Melting and refreezing in an ice shelf basal channel at the grounding line of the Kamb Ice Stream, West Antarctica. *J. Geophys. Res.*, 127(11), <https://doi.org/10.1029/2021JF006532>, 2022.
- 810 Wright, A., & Siegert, M.: A fourth inventory of Antarctic subglacial lakes. *Ant. Sci.* 24(6), 659-664. <https://doi.org/10.1017/S095410201200048X>, 2012.
- Zwally, H. J., Schutz, B., Abdalati, W., Abshire, J., Bentley, C., Brenner, A., Bufton, J., Dezio, J., Hancock, D., Harding, D., Herring, T., Minster, B., Quinn, K., Palm, S., Spinhirne, J., and Thomas, R.: ICESat's laser measurements of polar ice, atmosphere, ocean, and land, *J. Geodyn.*, 34, 405–445, [https://doi.org/10.1016/S0264-3707\(02\)00042-X](https://doi.org/10.1016/S0264-3707(02)00042-X), 2002.